Spectroscopic Measurements of Temperature and Plasma Impurity Concentration During Magnetic Reconnection at the Swarthmore Spheromak Experiment

Vernon H. Chaplin, Michael R. Brown, David H. Cohen, and Tim Gray

Department of Physics and Astronomy, Swarthmore College, Swarthmore, Pennsylvania 19081

Chris D. Cothran

Department of Physics and Astronomy, Swarthmore College, Swarthmore, Pennsylvania 19081 and
Department of Physics and Astronomy, Haverford College, Haverford, Pennsylvania 19041

Temperature measurements during counter-helicity spheromak merging studies at the Swarthmore Spheromak Experiment (SSX) [M. R. Brown, Phys. Plasmas **6**, 1717 (1999)] are presented. VUV monochromator measurements of impurity emission lines are compared with model spectra produced by the non-LTE excitation kinematics code PrismSPECT [J. J. MacFarlane *et al.*, in *Proc. of the Third Conf. on Inertial Fusion Science and Applications* (2004)] to yield the electron temperature in the plasma with 1 μs time resolution. T_e is seen to increase from 20 eV to $30 - 35$ eV during spheromak merging. C III ion temperature, measured with an ion Doppler spectrometer (IDS) [C. D. Cothran *et al.*, Rev. Sci. Instrum. **77**, 063504 (2006)], likewise rises during magnetic reconnection but peaks at only 20-25 eV. The VUV emission line measurements are also used to constrain the concentrations of various impurities in the SSX plasma, which appear to be dominated by carbon. We conclude with an update on the progress of independent measurements of T_e using a four-filter soft x-ray detector in conjunction with PrismSPECT.
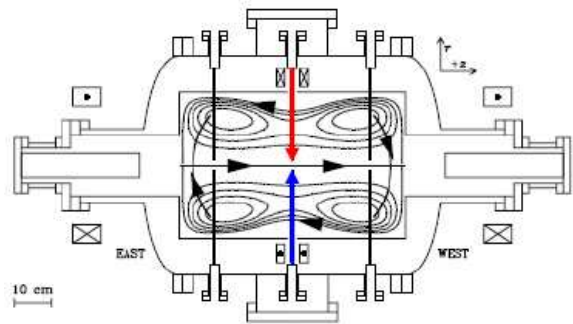
FIG. 1: Schematic of the SSX, shown in cross-section. The device is cylindrically symmetric about the horizontal axis in the figure. Spheromak plasmas are formed in the guns on the east and west sides of the vacuum chamber and ejected into the main flux conserver. The arrows represent the lines of sight of the VUV monochromator (red), and the soft x-ray detector and ion Doppler spectrometer (blue). Arrays of magnetic probes are shown schematically as four black lines in the figure. The contours represent the magnetic field lines of an FRC, the plasma structure that forms when two counter-helicity spheromaks merge. Figure modified from [6].

I. INTRODUCTION

Magnetic reconnection is the process driving the dynamics in spheromak merging and relaxation [1] as well as in several astrophysical scenarios [2]. During reconnection, magnetic energy is rapidly converted to electron and ion heat, plasma flow, and energetic particle beams [3, 4]. However, the partitioning of energy among various channels is not fully understood. Spheromak dynamics have been studied at the Swarthmore Spheromak Experiment (SSX) in a number of geometries [2, 5–8]. We have recently been studying spheromak merging in a prolate 0.4 m diameter, 0.6 m length, 3 mm wall copper flux conserver at SSX (see Fig. 1). In these experiments, merging of a pair of counter-helicity spheromaks generates magnetic reconnection dynamics near the midplane.

Local and global magnetic structure of SSX spheromaks has been studied with up to 600 individual internal magnetic probes operated simultaneously at 1.25 MHz using a multiplexer system [9]. Line averaged electron density is monitored with a quadrature HeNe laser interferometer [3]. We can scan density in a range $n_e = 1 - 10 \times 10^{14}$ cm^{-3}, and find a typical value of $n_e = 5 \times 10^{14}$ cm^{-3}. The composition of the SSX plasma is primarily hydrogen, with trace concentrations of carbon, oxygen, and other impurities. The plasma is fully ionized and fully magnetized, with typical magnetic fields of 0.1 T and an ion gyroradius, $\rho_i \ll R$, where $R = 0.2 - 0.25$ m is the outer flux conserving boundary of the plasma (defined by a cylindrical copper wall). The Lundquist number S, the ratio of the resistive magnetic diffusion time τ_R to the Alfvén transit time τ_A, is large for SSX, $S \approx 1000$. Accordingly, the global structure of SSX spheromaks is fully in the magnetohydrodynamic (MHD) regime ($S \gg 1, \rho_i \ll R$). Previous studies have constrained the plasma temperatures $T_e \approx T_i \leq 100$ eV [6, 10, 11].

Because magnetic reconnection is dynamically three-dimensional, it is often difficult to experimentally or observationally identify the reconnection site within the experimental volume or to determine whether the reconnection process has convected into the line of sight. In the experiments reported here, spectroscopic data are line-integrated over a 1 cm wide chord through a diameter at the midplane with a time resolution of about 1 μs. In addition, an ensemble of 20-30 discharges are typically

averaged for each measurement.

Line averaged electron temperature and impurity concentration levels are inferred from model fits to data from a vacuum ultraviolet (VUV) spectrometer. Data are analyzed with a non-LTE excitation/ionization kinematics code. This modeling is also used to explore the extent to which time-dependent, non-equilibrium excitation and ionization has to be accounted for. Ion temperature is measured with an ion Doppler spectrometer (IDS) [11]. We observe increases in both T_e and T_i during counter helicity spheromak merging, with the electron temperature approximately 10 eV higher than the ion temperature on average. We discuss possible physical and non-physical causes for this disparity in section IV.

In section II, details of the spectral modeling using the PrismSPECT code are presented. In section III, determinations of impurity concentration from the VUV spectrometer are presented. In section IV, we present measurements of the plasma electron temperature made using carbon emission line intensity ratios and compare these results with C III ion temperatures measured with IDS. In section V, we discuss the progress of additional elecron temperature measurements utilizing model fits to data from a four-channel soft x-ray (SXR) array. A summary is presented in section VI.

II. SPECTRAL MODELING

A. PrismSPECT

We analyzed the SXR and VUV data using the PrismSPECT non-LTE excitation/ionization code [12, 13]. Simulations were run for spatially uniform plasmas with a variety of temperatures, densities, and compositions. Model spectra and line strength ratios from these simulations were compared to spectroscopic data from SSX to determine best fit values for the plasma parameters of interest. We also used time-dependent simulations to study the plasma's approach to ionization/excitation equilibrium after spheromak formation.

PrismSPECT models all significant radiative and collisional (including three-body) processes, though not charge exchange. In its time dependent mode, the code computes atomic level populations at each time step by integrating the relevant rate equations forward in time, and the calculated level populations and transition probabilities are used to produce a model spectrum. In the steady-state mode, equilibrium ionization balances and level populations are calculated by inverting a rate matrix. In both modes, emissivities are calculated from the level populations and the emitted spectra are transported through the plasma, taking optical depth effects into account. Doppler shifts from bulk motion are not accounted for in PrismSpect, but all relevant line-broadening mechanisms – including the effects of natural, Stark, and thermal broadening – are accounted for [14].
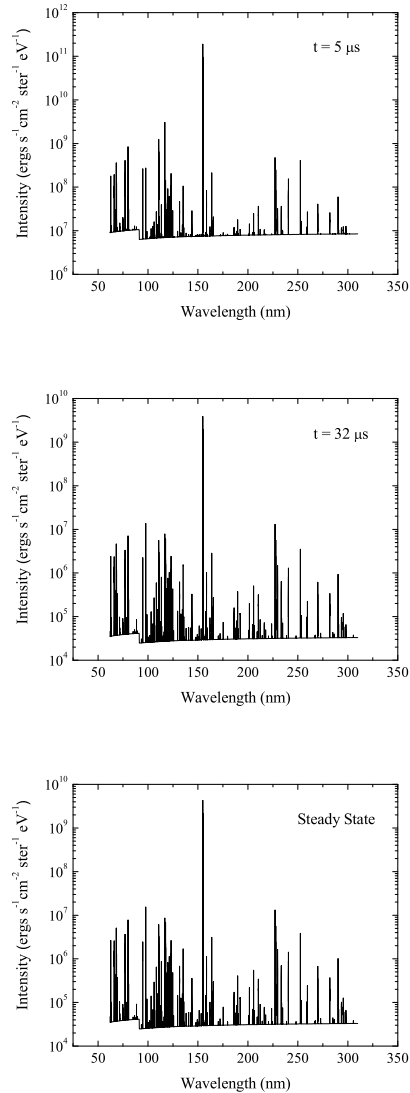

FIG. 2: Comparison of spectra from a 30 eV time-dependent simulation (top two panels) with a 30 eV steady-state spectrum (bottom panel). The ion density in the time dependent simulation was 8×10^{15} ions cm^{-3} during the first 10 μs (a typical value for the SSX plasma in the gun), decreasing linearly to reach 5×10^{14} ions cm^{-3} (the same value used for the steady state simulation) at $t = 30$ μs. Initial atomic level populations were calculated based on LTE at 0.025 eV in the time-dependent simulation. The time-dependent spectrum at $t = 5$ μs already shares many qualitative features with the steady-state spectrum, and by $t = 32$ μs the two spectra are essentially indistinguishable.

Atomic models for PrismSPECT simulations are drawn from the ATBASE database [15]. Many of the higher energy levels of impurity ions in the SSX plasma produce no strong spectral features, so we were able to make simplifications to the full ATBASE models and reduce simulation runtimes without sacrificing accuracy.

Tests of a variety of atomic models revealed 200 energy levels per carbon ion and 50 levels per nitrogen ion to be sufficient, while the oxygen model used contained 50 levels for O III through O VII and one level for the other ions. Hydrogen in SSX is almost 100% ionized, and line radiation following recombination of protons and electrons was found to make only negligible contributions to SXR signals, so we used only the ground state of neutral hydrogen and ionized hydrogen in our atomic model for H. For each element, adding more levels per ion stage beyond these described above did not lead to any significant change in the calculated spectra.

B.   Equilibration Time

The spheromak formation and expansion phases of an SSX discharge are characterized by turbulence and rapidly changing temperatures and densities [5]. Although it is difficult to estimate the time-varying conditions at the beginning of a discharge with a high degree of precision, the plasma conditions should not be varying significantly as the spheromaks approach the midplane. Here we investigate the extent to which the plasma is in ionization and excitation equilibrium. If it is, then the time history of the spheromak plasma is not important, and its spectrum can be modeled with a simple collisional-radiative equilibrium approach, in which the density, temperature, and composition are the only important parameters.

Research at SSX focuses primarily on the merging of two spheromaks rather than on the spheromak formation process itself. The merging and associated reconnection generally occurs at about $t = 40$ μs and lasts for roughly 20 μs. The VUV monochromator and SXR view the plasma along fixed lines of sight through the midplane (see Fig. 1), so measured signals are typically zero for approximately the first 30 μs of a discharge and peak around $t = 50 - 60$ μs. Steady-state simulations will therefore be sufficient if they can accurately describe the conditions in the plasma at $t > 30$ μs.

To test this, we calculated the evolution of the excitation and ionization of a hydrogen plasma with trace levels of carbon, nitrogen, and oxygen for a set of assumed density and temperature values as a function of time, based on our estimates of the conditions before, during, and after spheromak formation. A variety of initial conditions were tested, with electron temperatures in the plasma gun ranging from 0.025 eV to 60 eV. We computed ultraviolet spectra as well as quantities such as the mean charge state at many times during these simulations, and saw that these tended to approach a steady state after ~ 10 μs. We then compared the spectra at late times, between 30 and 40 μs, with spectra calculated assuming equilibrium conditions.

Indeed, these late-time spectra are indistinguishable, as shown in Fig. 2. The time-dependent simulations rapidly approach equilibrium once the plasma has ex-
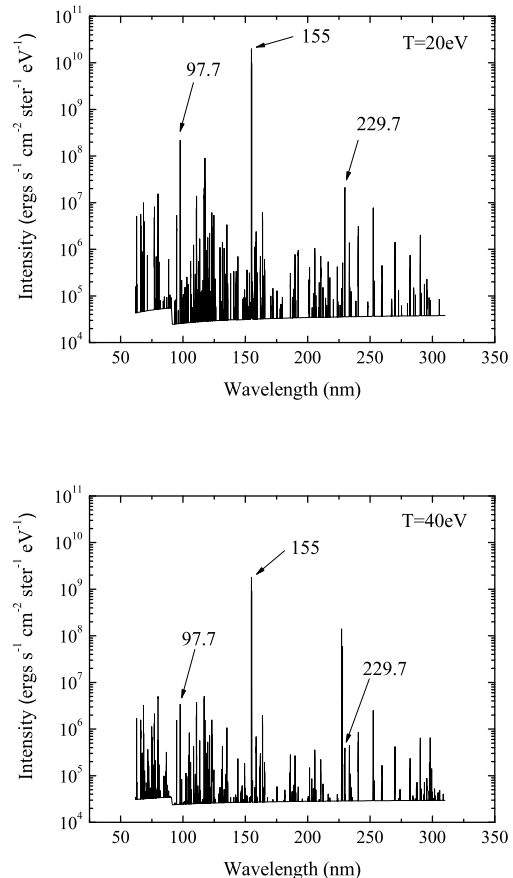

FIG. 3: Model spectra from steady-state simulations with T_e = 20 eV (top) and T_e = 40 eV (bottom). Both simulations assume a uniform 40 cm thick plasma composed of 99% hydrogen and 1% carbon with an ion density of 5×10^{14} cm^{-3}. The temperature dependence of the $I_{97.7}/I_{155}$ line ratio is evident. Note also the presence of the Lyman edge at 91.2 nm, indicating that radiative recombination of hydrogen, rather than bremsstrahlung, is the dominant continuum process at work.

panded to fill the flux conserver. We can explore this numerical result analytically. Using the expression for the collisional excitation cross section [16], we find the mean excitation time in SSX with $n_i = 5 \times 10^{14}$ ions cm^{-3} and $T_e = 30$ eV to be:

$$t \sim \frac{\sqrt{3kTm_e^3}}{n\pi\hbar^2} \sim 2 \times 10^{-7} \text{ s.} \qquad (1)$$

Therefore, in a period of several μs, each ion in SSX will be collisionally excited many times, indicating that equilibrium will be reached on a time scale (< 10 μs) that is short relative to the plasma lifetime, consistent with the detailed simulations which show little time-dependence after ~ 10 μs. Based on the observed insensitivity of late-time simulation results to initial conditions, tested

for a range of initial temperatures and atomic level populations, we conclude that we can safely use steady-state simulations to model the VUV and SXR spectra.
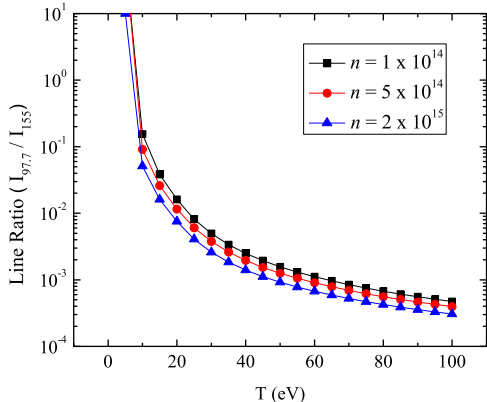
C. Line Ratio Modeling

FIG. 4: Simulated $I_{97.7}/I_{155}$ line ratio plotted as a function of temperature for three different plasma densities (given in cm^{-3}). Note the mild density dependence of this line ratio.

The SSX plasma, in the time leading up to reconnection, should be in coronal equilibrium, in which all upward atomic transitions are assumed to be caused by collisions between ions and electrons, and all downward transitions are assumed to occur by spontaneous emission. Similarly, ionization is by electron impact and is assumed to be balanced by radiative recombination. Since collisional ionization and radiative recombination both scale with the square of the plasma density, the overall ionization balance in a coronal plasma is density independent, and the ratio of the intensities of two lines from different ionization stages of the same element can serve as an electron temperature diagnostic. The primary line ratio used for our temperature determinations was C III 97.7 nm / C IV 155 nm (hereafter written as $I_{97.7}/I_{155}$). Representative spectra, calculated for two different temperatures, are shown in Fig. 3, where these two carbon lines are prominent.

The SSX plasma is essentially coronal; however, we ran simulations that included the full range of atomic processes and found a noticeable, though not major, density dependence in the $I_{97.7}/I_{155}$ ratio in the relevant density and temperature regimes (see Fig. 4). Although the deviation from coronal equilibrium is slight, C III and C IV are subdominant ion stages at T > 10 eV (see Fig. 5), so small absolute changes in their abundances can lead to large relative changes in the corresponding line intensity ratio. Because of this effect, it was necessary to obtain independent density measurements in order to use line ratios for precise calculations of electron temperature.
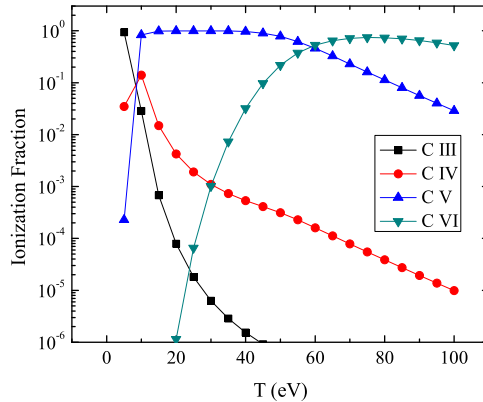

FIG. 5: Carbon ionization balance vs. electron temperature for an electron density of 5×10^{14} cm^{-3}.

We use an electron density value of $n_e = 5 \times 10^{14}$ cm^{-3} based on measurements with the laser interferometer.

III. IMPURITY DETERMINATIONS FROM VUV LINE MEASUREMENTS

Individual emission line strengths are measured in SSX using a vacuum ultraviolet (VUV) monochromator with a focal length of 0.2 m. Photons enter the device through a slit of adjustable width and strike a reflective diffraction grating, which selects and refocuses a narrow bandwidth around the desired central wavelength. Light leaving the diffraction grating is directed through an exit slit of adjustable width and into an 800 V photomultiplier tube (PMT). 500 μm was found to be the optimal exit slit width, corresponding to a spectral resolution of 2 nm. Signals from the PMT pass through a Stanford Research Systems SR570 current amplifier and are registered at 10 ns intervals by an oscilloscope and transferred to a computer using LabView. Sample traces from individual discharges for two different lines are shown in Fig. 6.

A wavelength calibration curve for the monochromator was constructed by finding the wavelength of peak intensity of a number of impurity lines known to be visible in the SSX plasma (for example, lines that had been observed with ion Doppler spectroscopy). However, intensity calibration using a known plasma source has not been carried out. By slowly scanning across the wavelengths around each line, we have ensured that lines are correctly identified and that measurements are made at the line centers, but the possibility exists that a wavelength dependence in the monochromator's intensity calibration could systematically affect our line ratios.

PrismSPECT was used to identify the carbon, nitrogen, and oxygen lines most likely to be strong in SSX, and
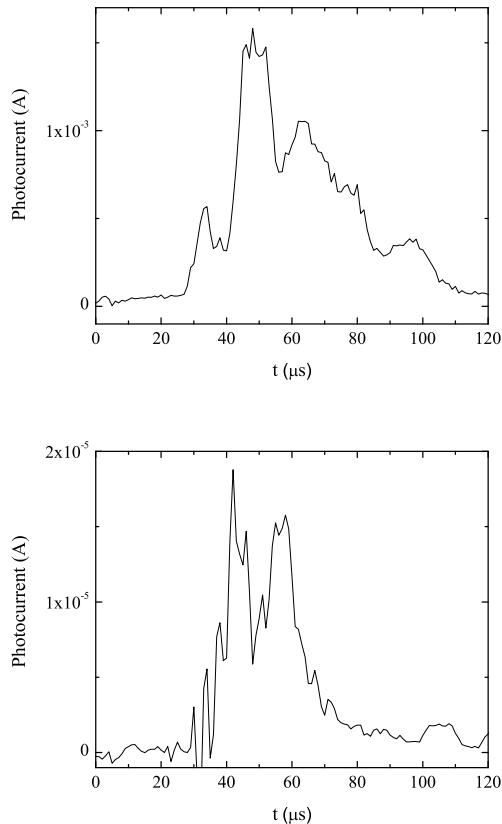
FIG. 6: Sample VUV monochromator data. Top: A measurement of the C III 97.7 nm line intensity during a single spheromak discharge in SSX. Bottom: A measurement of the C IV 155 nm line intensity during a discharge with counter-helicity spheromak merging.

TABLE I: Impurity Emission Lines Observed with the VUV monochromator.

Ion	λ (nm)	Transition	Typical Signal[a]
C III	97.7	$^1P_1 \rightarrow \, ^1S_0$	10 μA
C IV	155	$^2P_{1/2,3/2} \rightarrow \, ^2S_{1/2}$	1-2 mA
C V	227.4	$^3P_{0,1,2} \rightarrow \, ^3S_1$	not detected
C III	229.7	$^1D_2 \rightarrow \, ^1P_1$	10 μA
N IV	76.5	$^1P_1 \rightarrow \, ^1S_0$	not detected
N V	124	$^2P_{1/2,3/2} \rightarrow \, ^2S_{1/2}$	100 μA
O IV	55.4	$^2P_{1/2,3/2} \rightarrow \, ^2P_{1/2,3/2}$	not detected
O V	63.0	$^1P_1 \rightarrow \, ^1S_0$	5-10 μA
O VI	79	$^2D_{3/2,5/2} \rightarrow \, ^2P_{3/2}$	not detected
O VI	103.5	$^2P_{1/2,3/2} \rightarrow \, ^2S_{1/2}$	not detected

[a]Typical signals quoted are averaged over the 40-60 μs interval of each discharge.

we tuned the monochromator to observe these lines. The results are summarized in Tab. I. Five emission lines produced signals that could be reliably distinguished from background noise: C III 97.7 nm, C IV 155 nm, C III 229.7 nm, N IV 124 nm, and O V 63.0 nm. The strongest of these was C IV 155 nm, which consistently produced PMT currents over 1 mA. C V is the dominant carbon ionization stage at SSX temperatures (see Fig. 5); however, its resonance lines are outside the wavelength range accessible to the monochromator, so it is not necessarily surprising that no C V lines were detected.

The comparative strengths of C, N, and O lines can yield information about the relative fractions of these impurities present in SSX. These relative concentrations are a vital input for the simulations of soft x-ray spectra to be discussed in Section V. Of course, line ratios involving C, N, and O depend on temperature, the very parameter SXR is designed to constrain, so the problem is somewhat circular. Nevertheless, limits can be placed on relative impurity concentrations through comparisons of VUV line measurements with simulations.

We consider the ratios O V 63.0 nm / C III 97.7 nm and N IV 76.5 nm / C III 97.7 nm. All three lines arise from analogous atomic transitions (see Tab. I). As shown in Fig. 7, with equal concentrations of C and O present, the simulated $I_{63.0}/I_{97.7}$ ratio is $> 970/1$ for all plausible SSX temperatures. However, measured strengths of the two lines are approximately equal, implying that carbon is ~ 1000 times more abundant than oxygen in SSX. Likewise, the simulated $I_{76.5}/I_{97.7}$ ratio is $> 28/1$ for all plausible temperatures, while the VUV monochromator fails to detect N IV 76.5 nm. We therefore conclude that the nitrogen concentration in the SSX plasma is negligible.

It should be noted that strong signals were measured on most discharges for the N V 124 nm emission line. Contamination of the signal by the H Lyman alpha line at 121.6 nm is a possibility, although it seems unlikely given the reliability of our wavelength calibration curve at nearby wavelengths. Nevertheless, in the face of the conclusive non-detection of N IV 76.5 nm, confirmed by scanning over a range of energies around the expected wavelength, we feel it is safe to discard this measurement.

Stronger than expected signals were likewise observed for the C III 229.7 nm line. Simulated $I_{97.7}/I_{229.7}$ and $I_{155}/I_{229.7}$ ratios exceeded the measured ratios by over an order of magnitude. The 229.7 nm line is produced by an electron transition into the upper level of the 97.7 nm transition, so the observed ratio $I_{97.7}/I_{229.7} \sim 1$ could only occur if a substantial fraction of electrons were collisionally excited out of the 2p level before they had time to make the transition back to the ground state (see Fig. 8). We have yet to identify a likely mechanism by which this could occur. A strong 229.7 nm line has been independently observed in at least two other spheromaks [17, 18], although no publication we know of addresses the issue explicitly. In the case of SSX, we cannot rule out a misidentification of the line; the C V 227.4 nm line is expected to be strong at high temperatures (see Fig. 3),
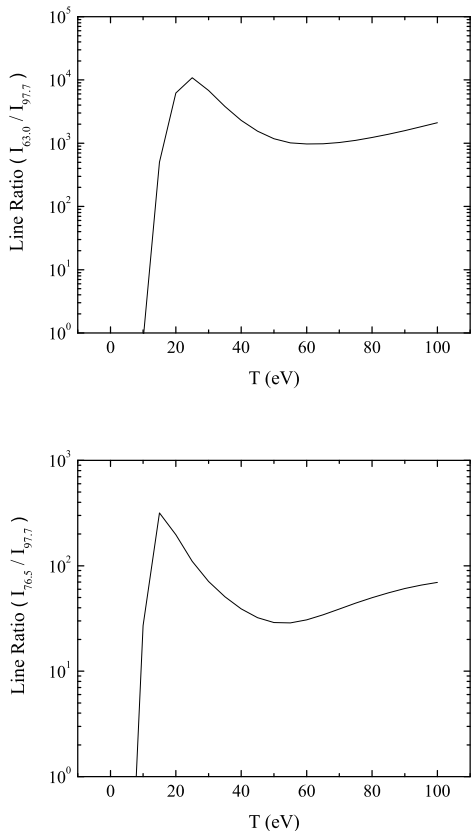
FIG. 7: Line ratios calculated from PrismSPECT simulations with 0.1% carbon, nitrogen, and oxygen impurities and $n_i = 5 \times 10^{14}$ cm^{-3}. The N IV 76.5 nm line is predicted to be over 28 times stronger than the C III 97.7 nm line for plausible SSX temperatures, and the O V 63.0 nm line is predicted to be over 970 times stronger. However, in the VUV monochromator data, the 97.7 nm and 63.0 nm line strengths are approximately equal, and the 76.5 nm line is not detected. These results allow us to place an upper limit on the concentrations of nitrogen and oxygen relative to carbon in the SSX plasma.

and we have not detected any other lines at $\lambda > 155$ nm that could be used to verify our wavelength calibration curve at long wavelengths.

IV. TEMPERATURE MEASUREMENTS

A. Electron Temperature

During the merging of two spheromaks, reconnection converts stored magnetic energy into thermal and kinetic energy. Understanding the details of this energy budget is vital for modeling coronal heating and other astrophysical phenomena. Electron temperatures during counter helicity spheromak merging were calculated by compar-
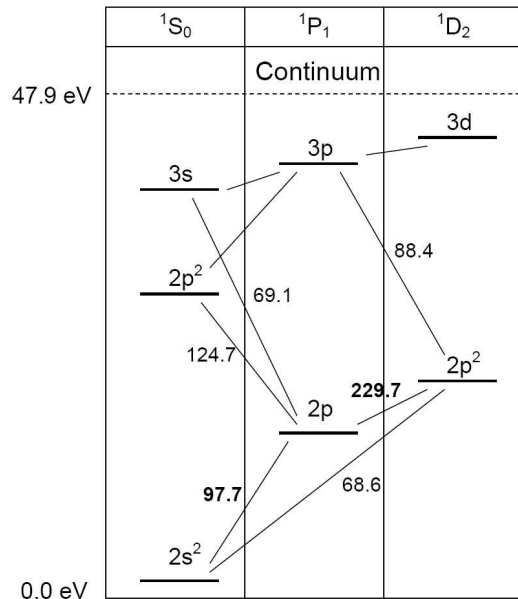

FIG. 8: Partial C III energy level diagram. Wavelengths corresponding to selected transitions are given in nm.

ing measured and simulated (Fig. 4) values of the carbon line ratio $I_{97.7}/I_{155}$. Models show that even the strongest emission lines in SSX are optically thin, so this comparison is quite straightforward. The results of the analysis of the $I_{97.7}/I_{155}$ ratio are shown in Fig. 9. T_e was also measured during single spheromak discharges, in which no magnetic reconnection took place.

The temperature during counter helicity discharges increases from 20 eV to 35 eV during the 35-70 μs time period (reconnection begins to occur at $t \sim 40$ μs), providing substantial evidence for magnetic energy being converted into heat. T_e rises rather gradually; however, we observe variations in the timing of the peak VUV monochromator signal for a given line from discharge to discharge, so more dramatic temperature spikes may have been smoothed over when the discharges were averaged together. A lesser temperature increase (~ 5 eV) is seen during single spheromak discharges, as the plasma relaxes into a lower-energy configuration around $t = 50$ μs. This measurement provides something of a control, indicating that the heating observed during reconnection is significant.

B. Ion Temperature

Ion temperature and flow dynamics are monitored at the midplane with an ion Doppler spectrometer (IDS). The SSX IDS instrument achieves high spectral resolution (0.0075 nm per pixel) and can measure the width and Doppler shift of impurity emission lines with 1 μs or better time resolution [11]. Fig. 10 shows the mean C III ion temperature during counter helicity merging, derived
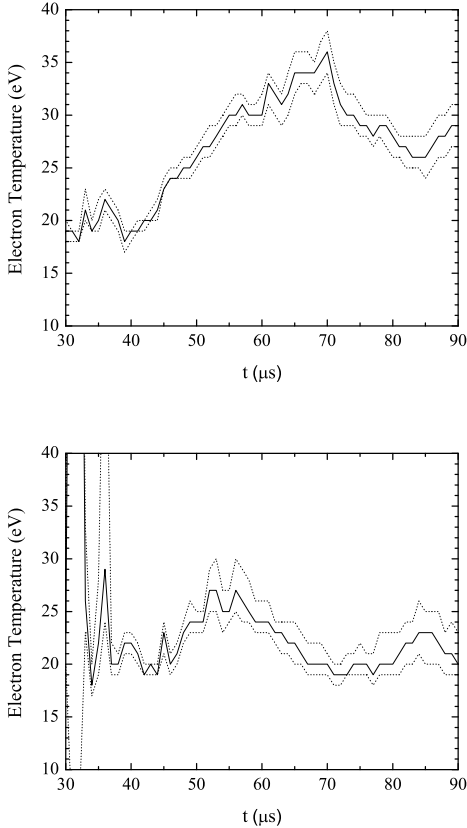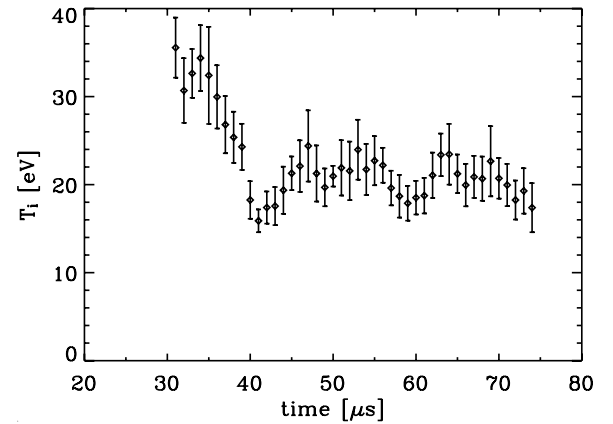
FIG. 10: Ion temperature during counter helicity merging calculated from IDS measurements of the C III 229.7 nm line. These temperatures represent the mean of ten separate discharges during which the IDS view chord was along a diameter through the midplane. The measurement shown is a direct characterization of the line width, which we attribute completely to thermal broadening. The data prior to ~ 40 μs show significant evidence for non-thermal broadening, thus we almost certainly overestimate T_i at early times. At later times, non-thermal contributions to the line width are negligible on average, so the ~ 10 eV increase in temperature after ~ 40 μs is likely due to heating from reconnection.

FIG. 9: Electron temperatures for counter helicity merging (top) and single spheromak discharges (bottom) derived from $I_{97.7}/I_{155}$ measurements averaged over 25 discharges for each line. An ion density of 5×10^{14} cm^{-3} was assumed. Dashed lines give the uncertainty range, defined as the temperatures implied by a line ratio one standard deviation above or below the mean.

from the second moment of the C III 229.7 nm lineshape data. Early time ($t < 40$ μs) results are likely unreliable due to low signal-to-noise ratio and non-thermal contributions to the line width. Starting at $t = 40$ μs, we measure a modest but significant T_i increase of 5-10 eV, with a peak C III temperature of ~ 25 eV.

As expected, we observe heating in both the electrons and ions during magnetic reconnection. However, the statistically significant difference in the peak temperatures ($T_e > T_i$ by ~ 10 eV) must be explained. We have yet to identify a detailed physical mechanism for preferential cooling of the ions or heating of the electrons, but such a process does not seem implausible. There could also be systematic errors in the measurements that we have not formally accounted for. As mentioned above, non-thermal broadening of the C III 229.7 nm line can lead us to overestimate T_i, but this effect would tend to increase the discrepency between T_e and T_i. A wavelength-dependence in the signal strength of

the VUV monochromator is certainly a possibly; between 97.7 nm and 155 nm the uncertainty is likely 10 % or less, corresponding to a shift in T_e of < 3 eV in the 20-40 eV range. Likewise, a factor of four uncertainty in the ion density would affect the calculated T_e by as much as 5 eV (see Fig. 4). We were unable to take data with the VUV monochromator and measure density with the interferometer simultaneously, so we cannot rule out this possibility with 100% certainty; however, interferometer data from other discharges suggests that n_i is constrained between 3×10^{14} cm^{-3} and 6×10^{14} cm^{-3} for all discharges with the standard gas valve delay. Therefore, the net effect of the aforementioned sources of systematic uncertainty on our T_e measurement should be no more than $\pm$ 5 eV. Referring back to Figs. 9 and 10, $T_e > T_i$ in SSX remains a noteworthy result, particularly at $t > 60$ μs.

V.   SXR MEASUREMENTS

The SSX soft x-ray detector (SXR) [6, 19–21] consists of a matched set of four International Radiation Detectors AXUV silicon p-n junction photodiodes filtered by thin films of aluminum (100 nm), titanium (50 nm), tin (100 nm), and zirconium (100 nm). The variation in the spectral response functions of the filters at EUV and soft x-ray energies (see Fig. 13) allows us to garner information about broad spectral properties with a time resolution of < 10 ns. Ultimately, we hope to use this data to supplement the VUV line ratio analysis and indepen-
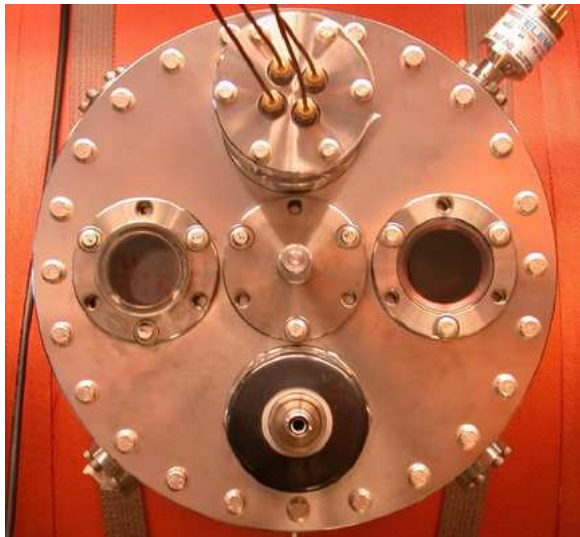
FIG. 11: Location of SXR at the midplane on the SSX machine (see the schematic in Fig. 1). The four wires at the top of the image carry current from the SXR photodiodes. Clockwise from upper left, the diodes are filtered by foils made of Al, Zr, Sn, and Ti. The port for the IDS is visible at the bottom center of this image.

FIG. 12: Model spectrum from a steady-state simulation with $T_e = 30$ eV and $n_i = 5 \times 10^{14}$ cm^{-3}. Impurity concentrations of 1% carbon and 0.001% oxygen were included. The plasma emits primarily at $E < 150$ eV, but SXR will also measure substantial emission from the C V and C VI resonance lines between 300 and 400 eV.

dently derive the electron temperature in SSX. Such a measurment is desirable for several reasons. Although the analysis lacks the simplicity of the line ratio measurement, it has the distinct advantage of allowing us to determine electron temperatures for individual discharges, since the flux through all four filters can be measured simultaneously. In addition, the SXR is sensitive to signficantly higher energy photons than the VUV monochrometer, and thus can potentially measure emission from hotter plasma and even emission produced by a possible high-energy, non-Maxwellian component of the electron population. Finally, the simultaneous measurement of emission from many lines in each filter bandpass averages out uncertainties in individual model line intensities. Here we report on the progress of these measurements.

Despite the low spectral resolution of the device, detailed calculations of the electron temperature in the plasma should be possible with the aid of model spectra from PrismSPECT (see Fig. 12). Using the relative impurity concentrations inferred from line ratio measurements (Section III), we run simulations at a range of temperatures from 5 to 100 eV. Model spectra are multiplied by the SXR filter responsivities to determine the filter signals produced at each temperature. We compare the model filter ratios to those measured in SSX (see Fig. 14) to calculate best-fit electron temperatures in the plasma at 1 μs intervals (the use of ratios removes the need for knowledge of absolute impurity concentrations).

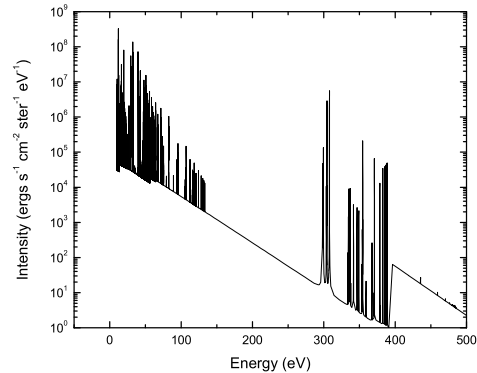Typical SXR measurements have shown significantly greater flux through the tin (Sn) filter than any other

filter (see Fig. 14), a result that is inconsistent with the known filter response functions between 10 and 500 eV (as is evident in Fig. 13). We tested for a leak below 10 eV by placing windows made of UV-fused silica (transmission cuts off abruptly above 7.3 eV [23]) and sapphire (transmission cuts off above 8.3 eV [24]) in the SXR line of sight. Signals from all four photodiodes with either of the windows in place were less than 2% of their unobscured values, ruling out significant low-energy transmission as a cause of the Sn filter anomaly. Future studies will continue to investigate this issue.

In the present research, we have discarded the Sn filter data and proceeded with electron temperature fitting using the ratios of signals from the other three filters. An example of the fitting process is shown in Fig. 15. Repeating this process at 1 μs intervals yields the evolution of T_e during the discharge. During typical discharges, we can achieve a good fit between the models and data at some time steps, but at other times the models do not fit the data well at any temperature. In this situation, the best-fit temperature calculated may not reflect the actual temperature in SSX, but rather trend systematically toward the locations of minima and maxima in the model curves shown in Fig. 15.

The lack of agreement between the models and data may be a sign that we have failed to include some of the necessary physics in our models. For example, a non-Maxwellian high-energy tail on the electron energy distribution would change the expected filter ratios at a given temperature, as would the presence of additional impurity species. SXR signals through all four filters increase significantly during reconnection and decay afterwards, suggesting that valuable information is contained in the data. The device has proven to be useful as a
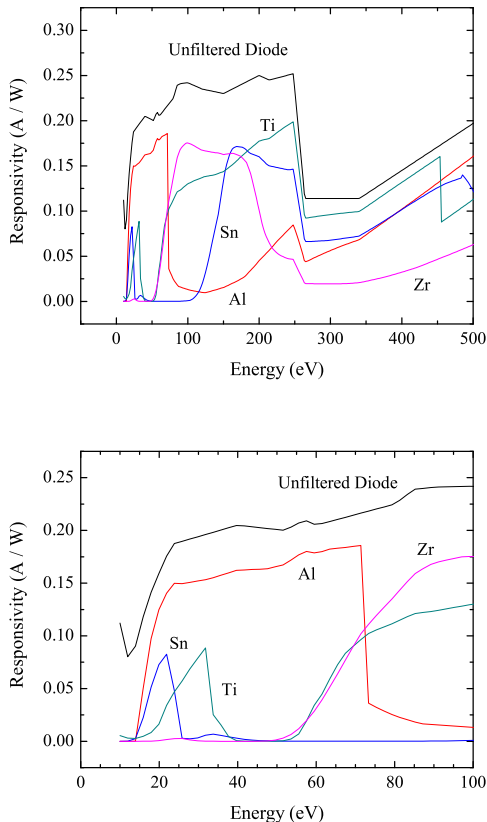
FIG. 13: SXR filter responsivities [22]. The colored lines show the response function of the filtered diodes in the 10 eV to 500 eV range, and the black line shows the response function of the unfiltered diode. Line emission at E > 500 eV was negligible at all simulation temperatures. The lower panel shows the same responsivity curves, but zoomed in on the range below 100 eV, where the bulk of the plasma emission is expected.

FIG. 14: Top: SXR data from a discharge with counter-helicity merging, smoothed over 1 μs intervals. Bottom: Time evolution of filter ratios for the discharge. Sn filter data is omitted in order to more clearly show the time evolution of the other three ratios.

probe into interesting and unexpected plasma properties, and it also shows promise as a temperature diagnostic, but more work is needed before reliable T_e measurements can be made. In particular, PrismSPECT models will be used to search for new filter materials that will allow us to better distinguish between different temperatures at $T_e > 50$ eV.

VI. SUMMARY

We have shown that high time resolution UV spectroscopy is a useful tool for characterizing the physical properties of the SSX plasma during and after magnetic reconnection. Electron temperature can be estimated analytically from impurity emission line ratios, but more precise measurements which take into account deviations from coronal equilibrium require detailed spectral modeling. This same modeling also shows that ionization and excitation equilibrium is reached within less than
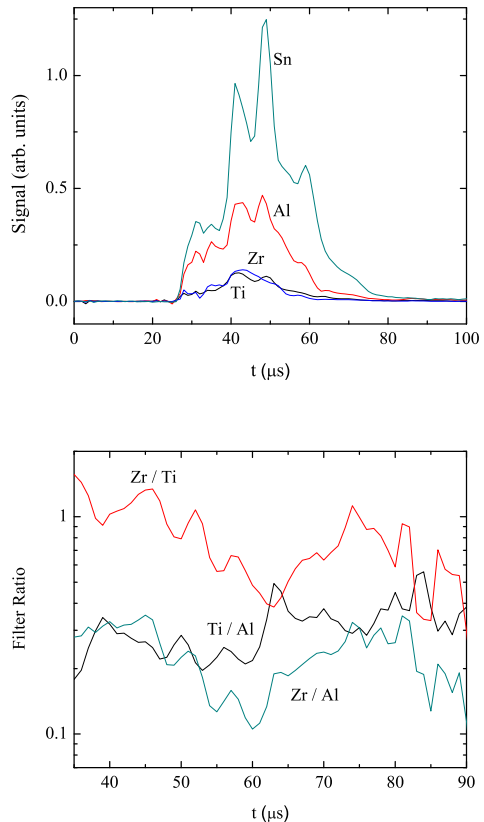
10 μs after the plasma is discharged from the guns, so that steady-state simulations are sufficient for describing the plasma emission at the time that reconnection occurs (~ 40 μs after the plasma discharge) and, furthermore, that the exact conditions in the plasma guns do not need to be known in order to accurately model the plasma properties around the time of reconnection.

Comparing model line ratios with measured UV line emission from various impurity species allows us to place constraints on the relative impurity concentrations in the plasma. Carbon is the dominant impurity in SSX, with a concentration approximately 1000 times greater than that of oxygen. Nitrogen is found to be at least two orders of magnitude less abundant than carbon. However, the concentration of carbon is high enough that line emission dominates continuum emission between 10 and 500 eV.

For the first time in SSX, we have made precise, high time resolution measurements of the electron temperature during counter helicity spheromak merging. Energy released by magnetic reconnection causes T_e to rise from approximately 20 eV to 35 eV on average during the 40-
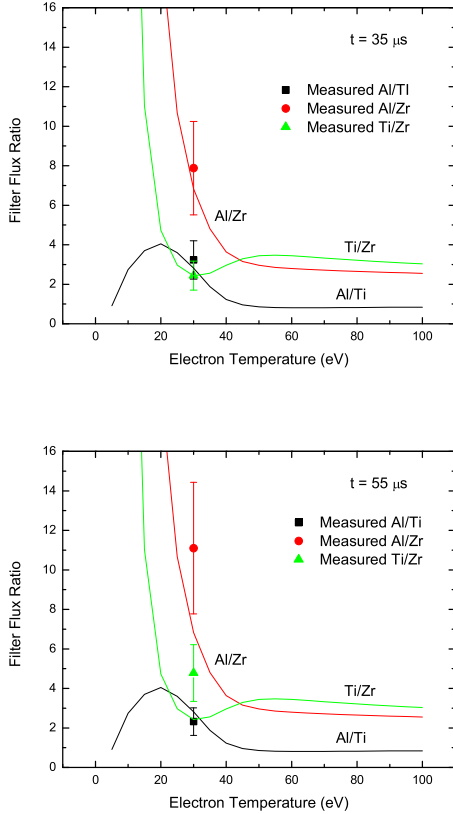
FIG. 15: Illustration of the process used to fit SXR data to model spectra and determine T_e. Filters ratios calculated from models are plotted as a function of temperature (solid lines). Measured filter ratios at $t = 35$ μs (top panel) and $t = 55$ μs (bottom panel) during a typical single spheromak discharge are plotted as points at the location of the calculated best-fit temperature for the time step. For illustrative purposes, 30% error in the measured ratios is assumed. At $t = 35$ μs, a good fit is achieved at $T = 30$ eV. However, at $t = 55$ μs, all three measured ratios cannot match the models at any one temperature, and the calculated best-fit temperature of 30 eV may not accurately reflect the actual T_e in the plasma.

70 μs interval of a discharge. Ion temperatures, as determined by line width measurements using an ion Doppler spectrometer, are approximately 10 eV lower. We have examined possible sources of systematic error and found that they are insufficient to explain the result $T_e > T_i$.

Utilizing the information about impurity concentrations derived from UV line intensity measurements, we have developed a framework for monitoring electron temperature during individual discharges using a broadband soft x-ray detector. Accurate modeling of the plasma conditions is crucial for the success of this technique, and the lack of consistent agreement thus far between measured and model SXR filter ratios may be a sign that we have not included all of the relevant physics in our simulations.

References

[1] M. R. Brown, Phys. Plasmas **6**, 1717 (1999).

[2] M. R. Brown, C. D. Cothran, and J. Fung, Phys. Plasmas **13**, 056503 (2006).

[3] M. R. Brown, C. D. Cothran, M. Landreman, D. Schlossberg, W. H. Matthaeus, G. Qin, V. S. Lukin, and T. Gray, Phys. Plasmas **9**, 2077 (2002).

[4] M. R. Brown, C. D. Cothran, M. Landreman, D. Schlossberg, W. H. Matthaeus, G. Qin, V. S. Lukin, and T. Gray, Astroph. Journal Lett. **577**, L63 (2002).

[5] C. G. R. Geddes, T. W. Kornack, and M. R. Brown, Phys. Plasmas **5**, 1027 (1998).

[6] C. D. Cothran, A. Falk, A. Fefferman, M. Landreman, and M. R. Brown, Phys. Plasmas **10**, 1748 (2003).

[7] C. D. Cothran, M. Landreman, M. R. Brown, and W. H. Matthaeus, Geophys. Res. Lett. **32**, L03105 (2005).

[8] M. R. Brown, C. D. Cothran, J. Fung, M. Chang, J. Horwitz, M. J. Schaffer, J. Leuer, and E. V. Belova, Phys. Plasmas **13**, 102503 (2006).

[9] M. Landreman, C. D. Cothran, M. R. Brown, M. Kostora, and J. T. Slough, Rev. Sci. Instrum. **74**, 2361 (2003).

[10] M. R. Brown, C. D. Cothran, D. H. Cohen, J. Horwitz, and V. Chaplin, **27**, 16 (2008).

[11] C. D. Cothran, J. Fung, M. R. Brown, and M. J. Schaffer, Rev. Sci. Instrum. **77**, 063504 (2006).

[12] Prism Computational Sciences, Inc., *PrismSPECT*, Spectral Analysis Code, www.prism-cs.com/Software/PrismSPECT/PrismSPECT.htm.

[13] J. J. MacFarlane, I. E. Golovkin, P. R. Woodruff, D. R. Welch, B. V. Oliver, T. A. Mehlhorn, and R. B. Campbell, in *Proceedings of the Third Conference on Inertial Fusion Science and Applications, Monterey, California*, edited by B. A. Hammel, D. D. Meyerhofer, J. M. ter Vehn, and H. Azechi (Am. Nuc. Soc., 2004).

[14] I. E. Golovkin, J. J. MacFarlane, P. Woodruff, J. E. Bailey, G. Rochau, K. Peterson, T. A. Mehlhorn, and R. C. Mancini, J. Quant. Spect. Rad. Transfer **99**, 199 (2006).

[15] Prism Computational Sciences, Inc., *Prism atomic physics data*, Prism Atomic Data, www.prism-cs.com/Software/AtomicData/AtomicData.htm.

[16] D. E. Osterbrock, *Astrophysics of Gaseous Nebulae and Active Galactic Nuclei* (University Science Books, Mill Valley, CA, 1989).

[17] W. C. Turner, G. C. Goldenbaum, E. H. A. Granneman, J. H. Hammer, C. W. Hartman, D. S. Prono, and J. Taska, Phys. Fluids **26** (1983).

[18] G. Cunningham, Plasma Phys. Control. Fusion **39**, 1339 (1997).

[19] J. F. Hansen, Ph.D. thesis, Caltech (2001).

[20] S. Hokin, R. Fonck, and P. Martin, Rev. Sci. Instruments **63** (1992).

[21] V. A. Soukhanovskii, D. Stutman, M. Iovea, M. Finkenthal, H. W. Moos, T. Munsat, B. Jones, D. Hoffman, R. Kaita, and R. Majeski, Rev. Sci. Instrum. **72** (2001).

[22] Lawrence Berkeley National Laboratory, *Filter transmission*, *X-Ray Interactions with Matter*, http://henke.lbl.gov/optical_constants/filter2.html.

[23] Melles Griot, *Synthetic fused silica*, *Material Properties*, www.mellesgriot.com/pdf/CatalogX/X_04_11-13.pdf.

[24] Melles Griot, *Sapphire*, *Material Properties*, www.mellesgriot.com/pdf/CatalogX/X_04_16.pdf.